A&A 548, A71 (2012)
DOI: 10.1051/0004-6361/201220033

Astronomy & Astrophysics

Rotational spectrum of formamide up to 1 THz and first ISM detection of its ν_{12} vibrational state⋆

R. A. Motiyenko[1], B. Tercero[2], J. Cernicharo[2], and L. Margulès[1]

[1] Laboratoire de Physique des Lasers, Atomes, et Molécules, UMR CNRS 8523, Université de Lille 1, 59655 Villeneuve d'Ascq Cedex, France
e-mail: roman.motienko@univ-lille1.fr
[2] Centro de Astrobiología (CSIC-INTA), Laboratory of Molecular Astrophysics, Department of Astrophysics, Ctra de Ajalvir, Km 4, 28850 Torrejón de Ardoz, Madrid, Spain

Received 17 July 2012 / Accepted 21 September 2012

ABSTRACT

Context. Formamide is the simplest bearer of peptide bond detected in the interstellar medium (ISM).
Aims. There is still a lack of laboratory data on its rotational spectrum in the THz domain.
Methods. We measured the rotational spectrum of formamide in the frequency range 400–950 GHz. The ground and first excited vibrational state of the normal species as well as the ground state of ^{13}C isotopic species were analysed.
Results. The results obtained represent an extension by a factor of two in frequency range compared to previous studies. Of all transition frequencies in the dataset about 45% are new measurements. A reliable set of rotational constants allows accurate predictions of transition frequencies in the THz domain. Based on the spectroscopic results, the $\nu_{12} = 1$ excited vibrational state of formamide was detected in the IRAM 30 m line survey of Orion KL for the first time in the ISM.

Key words. line: identification – astronomical databases: miscellaneous – ISM: molecules – submillimeter: ISM – ISM: individual objects: Orion KL

1. Introduction

Formamide (NH_2CHO) has been established as an interstellar species back in the early 1970s (Rubin et al. 1971). It is an important molecule for interstellar pre-biotic chemistry because it contains a peptide bond –C(=O)NH– that holds together the chains of amino acids. Recently it has been shown that of all possible simplest interstellar molecules that contain a peptide bond, formamide is the most stable energetically (Lattelais et al. 2010). Formamide is a light molecule whose maximum absorption (emission) lies at about 650 GHz below 300 K and an intense spectrum that extends far beyond 1 THz. Several groups have studied the rotational spectrum of formamide since 1955 (Kurland 1955; Kurland & Bright Wilson 1957; Costain & Dowling 1960), but all these studies were quite limited in terms of frequency range. The first revision of the results made by Johnson et al. (1972) provided accurate predictions of transition frequencies of the ground state of formamide up to 180 GHz. Several subsequent studies (Kirchhoff & Johnson 1973; Hirota et al. 1974; Moskienko & Dyubko 1991; Vorob'eva & Dyubko 1994) have extended the measurements into the sub-millimeter wave range up to 445 GHz for the ground and first excited vibrational state ν_{12}. The recent paper by Kryvda et al. (2009) presents a new revision of all previous results as well as new spectroscopic data on normal, ^{13}C, ^{15}N, and ^{18}O isotopic species of formamide in the frequency range up to 250 GHz.

We report here on an extended study of the rotational spectrum of the ground and first excited vibrational state of normal formamide as well as on the ground state of $NH_2^{13}CHO$ in the frequency range 400–950 GHz. We also report the first detection of the $\nu_{12} = 1$ state in Orion KL, which is based on improved spectroscopic data obtained in this study.

2. Experiments

The measurements of the rotational spectrum of formamide were performed in three frequency windows: 400–465 and 800–945 GHz with a solide-state source spectrometer (Motiyenko et al. 2010); and 580–660 GHz with a fast-scan spectrometer (Alekseev et al. 2012). The sample of NH_2CHO of 99% purity was purchased at Aldrich and was used without further purification. Thus, the spectra of ^{13}C isotopic species of formamide were measured in natural abundance (about 1.1%). The optimum sample pressure was found to be about 1 Pa (10 μbar) with a tendency to increase to 2 Pa at higher frequencies. The measurement accuracy for a strong isolated line is estimated to be better than 30 kHz in the frequency range up to 500 GHz and 50 kHz in the frequency range above 500 GHz due to Doppler line broadening. Blended lines and lines with a poor signal-to-noise ratio were weighted at 50 or 100 kHz, respectively.

3. Assignments and fit

Formamide is a prolate asymmetric top molecule, its asymmetry parameter is $\kappa = -0.95$. Theoretical and experimental studies suggest that formamide is an almost planar molecule with

⋆ Measured rotational transitions (Tables 4–6) are only available at the CDS via anonymous ftp to cdsarc.u-strasbg.fr (130.79.128.5) or via http://cdsarc.u-strasbg.fr/viz-bin/qcat?J/A+A/548/A71

Table 1. Rotational constants of formamide.

S-reduction		A-reduction			
Parameters	NH_2CHO $v = 0$	Parameters	NH_2CHO $v = 0$	NH_2CHO ν_{12}	$NH_2^{13}CHO$ $v = 0$
A (MHz)	72716.89840(19)[a]	A (MHz)	72716.89800(19)	71738.72306(35)	71058.2044(11)
B (MHz)	11373.509642(28)	B (MHz)	11373.582453(28)	11351.591159(46)	11372.56100(11)
C (MHz)	9833.952804(27)	C (MHz)	9833.881236(26)	9839.250469(44)	9801.88771(11)
D_J (kHz)	7.761879(23)	Δ_J (kHz)	7.985385(25)	8.045855(47)	7.92971(15)
D_{JK} (kHz)	–67.83261(43)	Δ_{JK} (kHz)	–69.17265(44)	–66.89468(83)	–68.7265(27)
D_K (kHz)	1400.6906(38)	Δ_K (kHz)	1401.8297(39)	1316.3907(55)	1391.412(54)
d_1 (kHz)	1.5757698(38)	δ_J (kHz)	1.5757972(33)	1.5649226(80)	1.603172(72)
d_2 (kHz)	0.1116821(18)	δ_K (kHz)	36.12735(46)	33.7255(12)	35.398(11)
H_J (Hz)	0.0093375(57)	Φ_J (Hz)	0.0109407(68)	0.010671(15)	0.010969(60)
H_{JK} (Hz)	–0.19637(18)	Φ_{JK} (Hz)	0.02458(46)	[0.0]	[0.0]
H_{KJ} (Hz)	–5.7948(20)	Φ_{KJ} (Hz)	–6.5546(25)	–6.0831(56)	–6.429(11)
H_K (Hz)	80.679(48)	Φ_K (Hz)	81.477(49)	67.948(44)	82.03(65)
h_1 (Hz)	0.0045512(18)	ϕ_J (Hz)	0.0047135(19)	0.0045954(44)	0.004926(36)
h_2 (Hz)	0.0008207(16)	ϕ_{JK} (Hz)	0.06666(42)	0.06623(88)	0.0549(63)
h_3 (Hz)	0.00017663(30)	ϕ_K (Hz)	12.506(21)	10.428(20)	11.155(63)
L_{JK} (mHz)	–0.01208(49)	L_{JK} (mHz)	–0.02370(49)	–0.0238(14)	[0.0]
L_{KKJ} (mHz)	0.4272(29)	L_{KKJ} (mHz)	0.4614(29)	0.398(11)	[0.0]
L_K (mHz)	–5.41(16)	L_K (mHz)	–6.25(16)	[0.0]	[0.0]
l_2 (mHz)	–0.00001296(26)	χ_{aa} (MHz)	1.9543(13)	1.7616(33)	1.9653(27)
χ_{aa} (MHz)	1.9544(12)	χ_{cc} (MHz)	–3.8511(11)	–3.5823(16)	–3.8631(29)
χ_{cc} (MHz)	–3.8510(11)				
N[b]	1630(709)		1630(709)	1243(581)	409(190)
σ (MHz)[c]	0.029		0.028	0.029	0.029
σ_w[d]	0.72		0.72	0.70	0.70
$J_{\rm Max}, K_{a,\rm Max}$	65, 24		65, 24	63, 22	45, 15

Notes. [(a)] Numbers in parenthesis are one time the standard deviation. [(b)] Number of distinct frequency lines in fit. Number in parenthesis corresponds to new measurements. [(c)] Standard deviation of the fit. [(d)] Weighted deviation of fit.

an amino group with a slightly pyramidal structure. The amino group also exhibits extreme flexibility and its out-of-plane wagging is the lowest vibrational mode (ν_{12} = 289 cm^{-1}). All other excited vibrational states lie above 500 cm^{-1} and, consequently, would hardly represent an interest for astrophysical observations. The rotational spectrum of formamide is dominated by a strong series of a-type transitions owing to the high value of the μ_a dipole moment projection (μ_a = 2.7 D) and the relatively weak series of b-type transitions (μ_b = 0.8 D). Another particular feature of the rotational spectrum of formamide is the ^{14}N nuclear quadrupole hyperfine structure. In a Doppler limited resolution it can be observed for transitions with relatively low J and K_a values. In our measurements, hyperfine splittings were observed for some weak b-type transitions even at 850 GHz.

The assignment process based on predictions available from recent studies (Kryvda et al. 2009) was rather straightforward and did not present any major difficulties. Relatively small deviations from the predicted frequencies were only observed for high K_a transitions of normal isotopologue and high J transitions of ^{13}C species. However, after they were added to dataset the transitions were fitted within experimental accuracy. The final dataset consists of 1630 transition frequencies of the ground state of normal species of formamide, 709 of which are new measurements. For the ν_{12} state and ^{13}C isotopic species the final datasets contain 1243(581) and 409(190) transition frequencies respectively, where the number of new measurements is indicated in parentheses.

In fitting the rotational spectra of the ground vibrational state we tested both the A- and S-reductions of the Watson Hamiltonian in I^r representation since the structure of the formamide molecule is rather close to the symmetric top (κ = −0.95). In this case, the choice of reduction is not obvious. The two reductions are distinguished first of all by a different definition of the s_{111} parameter of the transformation (reduction) operator. First, we performed ab initio calculations of the harmonic force field of formamide. Calculation were performed at the B3LYP level of theory (Becke 1988; Lee et al. 1988) and using a 6-311++G(3df, 2pd) basis set. From the results of the calculations we estimated the value of the s_{111} parameter for both reductions. Watson (see Watson 1977) showed that to ensure a fast convergence of the Hamiltonian, the parameter s_{111} should not exceed the order of magnitude of T/B, where T and B are the values of the quartic distortion constants and the corresponding rotational constants for the molecule in question. It appears that the value of the s_{111} parameter is much lower for the S-reduction ($s^{\rm A}_{111} = 2.8\times10^{-7}$, $s^{\rm S}_{111} = 2.7\times10^{-8}$). However both $s^{\rm A}_{111}$ and $s^{\rm S}_{111}$ are lower than any T/B (see Table A.1). Second, the results of the least-squares fits using the A- and S-reduction Hamiltonians are rather similar, as follows from their comparison in the Table 1. The only difference is the number of parameters used in each fit. For the available dataset, the fits of the same quality were obtained from the 18 parameters of the A-reduction and 19 parameters of the S-reduction Hamiltonian. Finally, we performed additional fits for transitions with unresolved hyperfine splittings to check the condition number of the system of normal equations. Here, for the fit with the A-reduction Hamiltonian the condition number $\eta_{\rm A}$ = 332 is somewhat higher than for the S-reduction $\eta_{\rm S}$ = 221.

In summary, both the A- and S-reductions of the Watson Hamiltonian can be used in fitting the rotational spectrum of

formamide. In our study we preferred using the A-reduction because it needs smaller number of parameters to be fitted. Therefore the analysis of the ground and $\nu_{12} = 1$ excited vibrational state and the ground state of ^{13}C isotopic species was performed with the A-reduction.

For the least-squares fitting and to predict the spectra, Pickett's SPFIT/SPCAT programs (Pickett 1991) were used. The additional statistical tests for transitions with unresolved hyperfine splittings were performed with the ASFIT program of Z. Kisiel[1]. These tests were also important in choosing a correct set of octic centrifugal distortion parameters. Compared to the last study we found that the non-diagonal octic parameter of the A-reduction l_K determined previously (Kryvda et al. 2009) deteriorates the conditionality of the fit. This can lead to large errors in predicting the transition frequencies, which are sensitive to this parameter. Taking the present set of rotational transitions into account, the best choice of octic parameters for the ground state consists of L_{JK}, L_{KKJ}, and L_K, which provides good conditionality and allows fitting the spectrum within the experimental accuracy. For the ν_{12} state, only L_{JK} and L_{KKJ} could be determined from the present dataset.

The sets of rotational and hyperfine constants determined in this study for the ground and ν_{12} states of NH_2CHO and for the ground state of $NH_2^{13}CHO$ are presented in Table 1. The complete list of the measured rotational transitions (Tables 4–6) is available at the CDS.

4. First detection of NH_2CHO $\nu_{12} = 1$ in Orion KL

We have detected vibrationally excited formamide for the first time in space in the IRAM 30 m line survey of Orion KL presented in Tercero et al. (2010, 2011a). After summarizing the observations, data reduction, and overall results of that line survey (Sects. 4.1 and 4.2), we concentrated on the detection of NH_2CHO $\nu_{12} = 1$ and its analysis (Sect. 4.3). Finaly, we derived vibrational temperatures (Sect. 4.4).

4.1. Observations and data reduction

The observations were carried out using the IRAM 30 m radio telescope during September 2004 (3 mm and 1.3 mm windows), March 2005 (full 2 mm window), April 2005 (completion of 3 mm and 1.3 mm windows), and January 2007 (maps and pointed observations at particular positions). Four SiS receivers operating at 3, 2, and 1.3 mm were used simultaneously with image sideband rejections within 20–27 dB (3 mm receivers), 12–16 dB (2 mm receivers) and ≃13 dB (1.3 mm receivers). System temperatures were in the range 100–350 K for the 3 mm receivers, 200–500 K for the 2 mm receivers, and 200–800 K for the 1.3 mm receivers, depending on the particular frequency, weather conditions, and source elevation. For frequencies in the range 172–178 GHz, the system temperature was significantly higher, 1000–4000 K, owing to the proximity of the atmospheric water line at 183.31 GHz. The intensity scale was calibrated using two absorbers at different temperatures and the atmospheric transmission model (ATM, Cernicharo 1985; Pardo et al. 2001).

Pointing and focus were regularly checked on the nearby quasars 0420-014 and 0528+134. Observations were made in the balanced wobbler-switching mode, with a wobbling frequency of 0.5 Hz and a beam throw in azimuth of ±240″. No contamination from the off-position affected our observations except for a marginal one at the lowest elevations (~25°) for molecules showing low J emission along the extended ridge.

Two filter banks with 512 × 1 MHz channels and a correlator providing two 512 MHz bandwidths and 1.25 MHz resolution were used as backends. We pointed towards the IRc2 source at $\alpha_{2000.0} = 5^h35^m14.5^s$, $\delta_{2000.0} = -5°22'30.0''$ (J2000.0).

For a more detailed description of the observations and data reduction see Tercero et al. (2010).

4.2. Overall results of the line survey

Up-to-date overall results of the line survey: Within the 168 GHz bandwidth covered (80–115.5, 130–178, and 196–281 GHz), we detected more than 15 000 spectral features of which ~10 500 were already identified and attributed to 45 molecules, including 191 different isotopologues and vibrationally excited states. This paper is devoted to vibrationally excited formamide, therefore we do not extend our overall results here. We expect to publish our complete results by 2013; for more information, please contact J. C. and B. T. In Tercero et al. (2010) we described the line identification method for this line survey.

In agreement with previous works, four different spectral cloud components were defined in the analysis of the low angular resolution line surveys of Orion KL, where different physical components overlap in the beam. These components are characterized by different physical and chemical conditions (Blake et al. 1987, 1996; Tercero et al. 2010, 2011a): (i) a narrow or "spike" (~4 km s^{-1} line-width) component at $v_{LSR} \simeq 9$ km s^{-1} delineating a north-to-south *extended ridge* or ambient cloud ($T_k \simeq 60$ K, $n(H_2) \simeq 10^5$ cm^{-3}); (ii) a compact and quiescent region, the *compact ridge*, ($v_{LSR} \simeq 7-8$ km s^{-1}, $\Delta v \simeq 3$ km s^{-1}, $T_k \simeq 110$ K, $n(H_2) \simeq 10^6$ cm^{-3}) identified for the first time by Johansson et al. (1984); (iii) the *plateau*, a mixture of outflows, shocks, and interactions with the ambient cloud ($v_{LSR} \simeq$ 6–10 km s^{-1}, $\Delta v \gtrsim 25$ km s^{-1}, $T_k \simeq 150$ K, $n(H_2) \simeq 10^6$ cm^{-3}); (iv) a *hot core* component ($v_{LSR} \simeq 5$ km s^{-1}, $\Delta v \sim 10$ km s^{-1}, $T_k \simeq 250$ K, $n(H_2) \simeq 5 \times 10^7$ cm^{-3}) first detected in ammonia emission by Morris et al. (1980).

4.3. Detection and astronomical modelling

We detected formamide in the first vibrationally excited state through 55 emission lines of the line survey. Despite the large number of line blends in the 80–280 GHz domain, we were able to assign these 55 lines to NH_2CHO $\nu_{12} = 1$. Table 2 gives the observed line intensities and frequencies together with the predicted frequencies from the rotational constants, based on the work presented in this paper, for all transitions that are not strongly blended with other lines from other species. In these detections, we did not take into account the quadrupole hyperfine structure of the observed transitions due to the proximity in frequency of the splitted levels.

All emission lines expected to have a T_{MB} over 0.3 K (those lines that correspond with a-type transitions with $K_a \leq 2$, in the 1.3 mm domain) were detected. Unfortunately, several of them are blended with strong emission lines from other molecules; Table 2 gives information on these contaminating lines. There is no strong line expected that is not observed in the astronomical spectra. In addition, Table 2 gives the line intensity derived from the model predictions (see below). The observed brightness temperature for the lines in Table 2 was obtained from the peak emission channel in the spectra. To quantify the contribution of possible blending, all contaminating species should be

[1] See PROSPE web site: http://www.ifpan.edu.pl/~kisiel/prospe.htm

Table 2. Emission lines of NH_2CHO $\nu_{12} = 1$.

Transition J_{K_a,K_c}	Rest freq. (MHz)	E_u (K)	S_{ij}	Observed freq. (MHz)	Observed T_{MB} (K)	Modelled T_{MB} (K)
$4_{1,4}$–$3_{1,3}$	81 682.74	428.3	3.75	[1]	...	...
$4_{0,4}$–$3_{0,3}$	84 481.51	425.7	4.00	[2]	...	...
$4_{2,3}$–$3_{2,2}$	84 741.66	437.4	3.00	[3]	...	...
$4_{3,2}$–$3_{3,1}$	84 821.21	452.1	1.75	84 822.6	0.011	0.005
$4_{3,1}$–$3_{3,0}$	84 823.16	452.1	1.75	[4]	...	...
$4_{2,2}$–$3_{2,1}$	85 021.46	437.5	3.00	85 022.0	0.024	0.011
$4_{1,3}$–$3_{1,2}$	87 728.81	429.0	3.75	87 728.9	0.043	0.015
$5_{1,5}$–$4_{1,4}$	102 051.89	433.2	4.80	102 052.0	0.025	0.031
$5_{0,5}$–$4_{0,4}$	105 392.40	430.7	5.00	105 393.0	0.044	0.036
$5_{2,4}$–$4_{2,3}$	105 890.63	442.5	4.20	105 891.0	0.044	0.027
$5_{4,2}$–$4_{4,1}$	106 023.11	477.7	1.80	106 023.0	0.037	0.017
$5_{4,1}$–$4_{4,0}$	106 023.13	477.7	1.80	[4]	...	...
$5_{3,3}$–$4_{3,2}$	106 049.20	457.2	3.20	106 050.0	0.019	0.017
$5_{3,2}$–$4_{3,1}$	106 056.02	457.2	3.20	106 056.5	0.025	0.019
$5_{2,3}$–$4_{2,2}$	106 448.39	442.6	4.20	106 449.5	0.037	0.028
$5_{1,4}$–$4_{1,3}$	109 604.53	434.3	4.80	[5]	...	...
$6_{1,5}$–$5_{1,4}$	131 440.80	440.6	5.83	131 441.9[1]	0.091	0.070
$7_{0,7}$–$6_{0,6}$	146 786.16	443.8	6.99	146 785.8[7]	0.18	0.10
$7_{2,6}$–$6_{2,5}$	148 110.98	455.7	6.43	[8]	...	...
$7_{6,1}$–$6_{6,0}$	148 436.70	549.6	1.86	[9]	...	...
$7_{6,2}$–$6_{6,1}$	148 436.70	549.6	1.86	[4]	...	...
$7_{5,3}$–$6_{5,2}$	148 447.58	517.3	3.43	[10]	...	...
$7_{5,2}$–$6_{5,1}$	148 447.58	517.3	3.43	[4]	...	...
$7_{4,4}$–$6_{4,3}$	148 479.19	491.0	4.71	148 478.8[10]	0.15	0.091
$7_{4,3}$–$6_{4,2}$	148 479.57	491.0	4.71	[4]	...	...
$7_{3,5}$–$6_{3,4}$	148 546.28	470.4	5.71	[11]	...	...
$7_{3,4}$–$6_{3,3}$	148 587.08	470.4	5.71	[12]	...	...
$7_{2,5}$–$6_{2,4}$	149 649.30	455.9	6.43	149 649.7	0.13	0.091
$7_{1,6}$–$6_{1,5}$	153 227.92	447.9	6.85	153 226.8[11]	0.25	0.070
$8_{1,8}$–$7_{1,7}$	162 945.38	453.7	7.87	162 945.7	0.12	0.13
$8_{0,8}$–$7_{0,7}$	167 233.53	451.9	7.98	167 233.0	0.16	0.15
$8_{2,7}$–$7_{2,6}$	169 172.83	463.8	7.50	[10]	...	...
$8_{7,1}$–$7_{7,0}$	169 649.26	595.8	1.88	169 649.7	0.12	0.019
$8_{7,2}$–$7_{7,1}$	169 649.26	595.8	1.88	[4]	...	...
$8_{6,2}$–$7_{6,1}$	169 654.15	557.7	3.50	169 653.6	0.14	0.051
$8_{6,3}$–$7_{6,2}$	169 654.15	557.7	3.50	[4]	...	...
$8_{5,4}$–$7_{5,3}$	169 673.92	525.5	4.88	169 674.6[13]	0.30	0.092
$8_{5,3}$–$7_{5,2}$	169 673.93	525.5	4.88	[4]	...	...
$8_{4,5}$–$7_{4,4}$	169 723.79	499.1	6.00	[14]	...	...
$8_{4,4}$–$7_{4,3}$	169 724.82	499.1	6.00	[4]	...	...
$8_{3,6}$–$7_{3,5}$	169 816.46	478.6	6.87	169 816.6	0.23	0.10
$8_{3,5}$–$7_{3,4}$	169 897.86	478.6	6.87	[15]	...	...
$8_{2,6}$–$7_{2,5}$	171 448.53	464.1	7.50	171 449.3	0.19	0.13

Notes. Emission lines of NH_2CHO $\nu_{12} = 1$ present in the frequency range of the 30-m Orion KL survey that are not strongly blended with other lines from other species. Column 1 gives the line transition; Col. 2: calculated rest frequencies; Col. 3: energy of the upper level; Col. 4: line strength; Col. 5: observed frequencies assuming a v_{LSR} of 7.5 km s^{-1}; Col. 6: observed peak line temperature (see text, Sect. 4.3); Col. 7: modelled peak line temperature. Because of either their weakness or heavy blending, it is not possible to fit Gaussian profiles for these lines, so we cannot give an integrated intensity. Nevertheless, we assumed a line width of ≃4–7 km s^{-1} taking into account the channels involved in the considered features for the vibrationally excited formamide and the good agreement between model and observations (see text, Sect. 4.3).
(1) Blended with t-CH_3CH_2OH. (2) Blended with c-C_2H_4O. (3) Blended with CH_3OH and ^{30}SiO. (4) Blended with the last one. (5) Blended with HC_3N $\nu_7 = 1$. (6) Blended with CH_3CH_2CN b type. (7) Blended with $CH_3^{13}CH_2CN$. (8) Blended with CH_3OH. (9) Blended with $(CH_3)_2CO$. (10) Blended with U line. (11) Blended with CH_3OCOH. (12) Blended with CH_3OCOH and $^{13}CH_3OCOH$. (13) Blended with $^{13}CH_3CH_2CN$. (14) Blended with $O^{13}CS$. (15) Blended with CH_3OCH_3. (16) Noisy spectra due to the proximity of the atmospheric water line. (17) Blended with CH_2CHCN. (18) Blended with $H^{13}CCCN$ $\nu_7 = 1^-$. (19) Blended with CH_3CHO. (20) Blended with CH_3CHO and NH_2CHO. (21) Blended with $(CH_3)_2CO$ and HDCS. (22) Blended with CH_3CH_2CN out of plane torsion. (23) Blended with the blue wing of a SO_2 line. (24) Blended with the wings of some molecules such as CH_3OCOH and CH_3CH_2CN. (25) Blended with $^{34}SO_2$. (26) Blended with $CH_3O^{13}COH$. (27) Blended with CH_3OCOH and CH_3CH_2CN in the plane torsion. (28) Blended with CH_3CH_2CN in the plane torsion. (29) Blended with CH_3OCOD. (30) Blended with NH_2CHO and $SO_2\nu_2 = 1$. (31) Blended with $^{33}SO_2$. (32) Blended with SO. (33) Blended with CH_3OCOH and $^{13}CH_3OH$. (34) Blended with $H^{13}CCCN$ and ^{33}SO. (35) Blended with NH_2CHO and SO_2. (36) Blended with $CH_3{}^{13}CN$. (36) Blended with CH_3CN and $CH_3{}^{13}CN$. (38) Blended with CH_3CN. (39) Blended with NH_2CHO. (40) Blended with CH_3CN $\nu_8 = 1$. (41) Blended with CH_3CN $\nu_8 = 1$ and CH_2CHCN $\nu_{11} = 1$.

Table 2. continued.

Transition J_{K_a,K_c}	Rest freq. (MHz)	E_u (K)	S_{ij}	Observed freq. (MHz)	Observed $T_{\rm MB}$ (K)	Modelled $T_{\rm MB}$ (K)
$8_{1,7}$–$7_{1,6}$	174 955.20	456.3	7.87	174 955.8[16]	0.31	0.15
$10_{1,10}$–$9_{1,9}$	203 325.94	472.3	9.89	203 325.1	0.16	0.22
$10_{0,10}$–$9_{0,9}$	207 598.30	470.8	9.97	[17]	...	...
$10_{2,9}$–$9_{2,8}$	211 176.58	483.1	9.60	211 177.6	0.14	0.21
$10_{8,2}$–$9_{8,1}$	212 081.60	659.1	3.60	[10]	...	...
$10_{8,3}$–$9_{8,2}$	212 081.60	659.1	3.60	[4]	...	...
$10_{7,3}$–$9_{7,2}$	212 085.17	615.1	5.10	212 087.6[10]	0.12	0.065
$10_{7,4}$–$9_{7,3}$	212 085.17	615.1	5.10	[4]	...	...
$10_{9,2}$–$9_{9,1}$	212 088.01	708.8	1.90	[4]	...	...
$10_{9,1}$–$9_{9,0}$	212 088.01	708.8	1.90	[4]	...	...
$10_{6,5}$–$9_{6,4}$	212 104.28	577.1	6.40	212 105.1[18]	0.28	0.12
$10_{6,4}$–$9_{6,3}$	212 104.28	577.1	6.40	[4]	...	...
$10_{5,6}$–$9_{5,5}$	212 151.01	544.8	7.50	212 152.6[19]	0.45	0.19
$10_{5,5}$–$9_{5,4}$	212 151.06	544.8	7.50	[4]	...	...
$10_{4,7}$–$9_{4,6}$	212 253.57	518.5	8.40	[20]	...	...
$10_{4,6}$–$9_{4,5}$	212 258.90	518.5	8.40	[4]	...	...
$10_{3,8}$–$9_{3,7}$	212 395.88	498.0	9.10	212 396.3	0.22	0.17
$10_{3,7}$–$9_{3,6}$	212 649.64	498.0	9.10	212 647.6[21]	0.42	0.17
$10_{2,8}$–$9_{2,7}$	215 449.20	483.7	9.60	215 450.0[22]	0.25	0.21
$10_{1,9}$–$9_{1,8}$	218 181.67	476.2	9.89	218 182.6	0.26	0.23
$11_{1,11}$–$10_{1,10}$	223 445.71	483.0	10.9	223 446.3[23]	0.42	0.26
$11_{0,11}$–$10_{0,10}$	227 532.36	481.8	11.0	227 533.7[24]	0.72	0.27
$11_{2,10}$–$10_{2,9}$	232 109.57	494.3	10.6	232 110.0[7]	0.62	0.24
$11_{8,3}$–$10_{8,2}$	233 299.54	670.3	5.18	233 300.1[25]	0.32	0.048
$11_{8,4}$–$10_{8,3}$	233 299.54	670.3	5.18	[4]	...	...
$11_{9,2}$–$10_{9,1}$	233 302.95	720.0	3.64	233 304.0[26]	0.24	0.022
$11_{9,3}$–$10_{9,2}$	233 302.95	720.0	3.64	[4]	...	...
$11_{7,4}$–$10_{7,3}$	233 308.80	626.3	6.55	233 310.2[11]	0.33	0.091
$11_{7,5}$–$10_{7,4}$	233 308.80	626.3	6.55	[4]	...	...
$11_{10,1}$–$10_{10,0}$	233 315.20	775.5	1.91	233 315.2[11]	0.21	0.007
$11_{10,1}$–$10_{10,0}$	233 315.20	775.5	1.91	[4]	...	...
$11_{6,6}$–$10_{6,5}$	233 338.17	588.3	7.73	233 340.2[19]	0.19	0.15
$11_{6,5}$–$10_{6,4}$	233 338.17	588.3	7.73	[4]	...	...
$11_{5,7}$–$10_{5,6}$	233 403.69	556.0	8.73	233 395.2[27]	0.62	0.23
$11_{5,6}$–$10_{5,5}$	233 403.82	556.0	8.73	[4]	...	...
$11_{4,8}$–$10_{4,7}$	233 541.37	529.7	9.55	233 545.3[28]	0.53	0.16
$11_{4,7}$–$10_{4,6}$	233 552.01	529.7	9.55	233 552.7[10]	0.40	0.16
$11_{3,9}$–$10_{3,8}$	233 700.50	509.2	10.2	233 701.4	0.52	0.20
$11_{3,8}$–$10_{3,7}$	234 110.23	509.2	10.2	234 112.3[11]	0.61	0.21
$11_{2,9}$–$10_{2,8}$	237 623.00	495.2	10.6	[15]	...	...
$11_{1,10}$–$10_{1,9}$	239 653.46	487.7	10.9	239 655.0[29]	0.41	0.28
$12_{1,12}$–$11_{1,11}$	243 518.12	494.7	11.9	[30]	...	...
$12_{0,12}$–$11_{0,11}$	247 327.32	493.6	12.0	247 327.7	0.40	0.30
$12_{2,11}$–$11_{2,10}$	252 990.99	506.4	11.7	252 991.2[10]	0.72	0.27
$12_{9,3}$–$11_{9,2}$	254 519.63	732.2	5.25	[31]	...	...
$12_{9,4}$–$11_{9,3}$	254 519.63	732.2	5.25	[4]	...	...
$12_{8,4}$–$11_{8,3}$	254 520.26	682.5	6.67	[4]	...	...
$12_{8,5}$–$11_{8,4}$	254 520.26	682.5	6.67	[4]	...	...
$12_{10,2}$–$11_{10,1}$	254 529.91	787.7	3.67	[10]	...	...
$12_{10,3}$–$11_{10,2}$	254 529.91	787.7	3.67	[4]	...	...
$12_{7,5}$–$11_{7,4}$	254 536.75	638.6	7.92	[32]	...	...
$12_{7,6}$–$11_{7,5}$	254 536.75	638.6	7.92	[4]	...	...
$12_{7,5}$–$11_{7,4}$	254 536.75	638.6	7.92	[32]	...	...
$12_{11,1}$–$11_{11,0}$	254 548.28	849.1	1.92	[32]	...	...
$12_{11,2}$–$11_{11,1}$	254 548.28	849.1	1.92	[4]	...	...
$12_{6,7}$–$11_{6,6}$	254 578.76	600.5	9.00	[32]	...	...
$12_{6,6}$–$11_{6,5}$	254 578.76	600.5	9.00	[4]	...	...
$12_{5,8}$–$11_{5,7}$	254 667.08	568.3	9.92	[6]	...	...

Table 2. continued.

Transition J_{K_a,K_c}	Rest freq. (MHz)	E_u (K)	S_{ij}	Observed freq. (MHz)	Observed T_{MB} (K)	Modelled T_{MB} (K)
$12_{5,7}$–$11_{5,6}$	254 667.39	568.3	9.92	[4]	...	...
$12_{4,9}$–$11_{4,8}$	254 845.87	541.9	10.7	[33]	...	...
$12_{4,8}$–$11_{4,7}$	254 865.75	541.9	10.7	254 866.2	0.28	0.18
$12_{3,10}$–$11_{3,9}$	255 010.36	521.4	11.2	255 011.4	0.30	0.23
$12_{3,9}$–$11_{3,8}$	255 642.37	521.4	11.2	[34]	...	...
$12_{2,10}$–$11_{2,9}$	259 878.29	507.6	11.7	[28]	...	...
$12_{1,11}$–$11_{1,10}$	261 010.66	500.3	11.9	261 010.2[10]	0.54	0.31
$13_{1,13}$–$12_{1,12}$	263 544.02	507.3	12.9	[35]	...	...
$13_{0,13}$–$12_{0,12}$	267 010.81	506.4	12.9	267 012.1	0.40	0.33
$13_{2,12}$–$12_{2,11}$	273 816.96	519.5	12.7	273 817.1	0.48	0.30
$13_{9,4}$–$12_{9,3}$	275 738.22	745.4	6.77	[15]	...	...
$13_{9,5}$–$12_{9,4}$	275 738.22	745.4	6.77	[4]	...	...
$13_{8,5}$–$12_{8,4}$	275 744.01	695.7	8.08	[15]	...	...
$13_{8,6}$–$12_{8,5}$	275 744.01	695.7	8.08	[4]	...	...
$13_{10,3}$–$12_{10,2}$	275 745.71	801.0	5.31	[15]	...	...
$13_{10,4}$–$12_{10,3}$	275 745.71	801.0	5.31	[4]	...	...
$13_{11,2}$–$12_{11,1}$	275 762.94	862.3	3.69	[36]	...	...
$13_{11,3}$–$12_{11,2}$	275 762.94	862.3	3.69	[4]	...	...
$13_{7,6}$–$12_{7,5}$	275 769.39	651.8	9.23	[37]	...	...
$13_{7,7}$–$12_{7,6}$	275 769.39	651.8	9.23	[4]	...	...
$13_{12,1}$–$12_{12,0}$	275 787.77	929.4	1.92	[37]	...	...
$13_{12,2}$–$12_{12,1}$	275 787.77	929.4	1.92	[4]	...	...
$13_{6,8}$–$12_{6,7}$	275 826.65	613.7	10.2	[38]	...	..
$13_{6,7}$–$12_{6,6}$	275 826.66	613.7	10.2	[4]	...	...
$13_{5,9}$–$12_{5,8}$	275 942.13	581.5	11.1	275 942.1	0.27	0.29
$13_{5,8}$–$12_{5,7}$	275 942.78	581.5	11.1	[4]	...	...
$13_{4,10}$–$12_{4,9}$	276 167.82	555.2	11.8	[39]	...	...
$13_{4,9}$–$12_{4,8}$	276 203.04	555.2	11.8	[40]	...	...
$13_{3,11}$–$12_{3,10}$	276 320.81	534.7	12.3	[41]	...	...
$13_{3,10}$–$12_{3,9}$	277 258.54	534.8	12.3	277 259.9	0.34	0.26

modelled. Hence, we limited ourselves in Table 2 to those lines that are practically free of blending or that only are affected by other weak lines. Consequently, our observed main-beam temperatures have to be considered as upper limits for these weakly blended lines. The predicted intensities agree quite well with the observations of 55 spectral lines detected, with 26 lines practically free of blending with other species. All together these observations ensure the detection of NH_2CHO $\nu_{12} = 1$ in Orion KL.

Figure 1 shows selected detected lines at 3, 2, and 1.3 mm, together with our best model (see below). The figure shows 26 detected lines without blending with other species, which support the first detection in space of NH_2CHO $\nu_{12} = 1$. The overlaps with other species are quoted in Table 2.

Figure 2 shows emission lines of formamide in the ground state present in our survey that are not strongly blended with other species together with our best model (see next paragraphs). To fit the emission lines of formamide (ground state and vibrationally excited), we found that only the compact ridge (C.R.) and the hot core (H.C.) components are needed to reproduce the line profiles. Nevertheless, the peak velocity of the emission lines (ground and vibrationally excited state) corresponds with the value associated with the compact ridge. For that reason a radial velocity of 7.5 km s^{-1} (see parameters for the compact ridge component quoted in Sect. 4.2) is assumed for the observed frequencies given in Table 2 and Figs. 1 and 2. We note that the line widths (for formamide in the ground state) vary between 4 to 7 km s^{-1} from the lower frequencies (observed lines more affected by the colder component of the compact ridge with $\Delta v \simeq 4$ km s^{-1}) to the higher ones (at 1.3 mm the line profiles show the contribution of the hot core component with $\Delta v \simeq 15$ km s^{-1}; 7 km s^{-1} of line width is the result of the blend of both components). Despite of either the weakness or heavy blending of the observed lines attributed to vibrationally excited formamide, the line widths of these features seem to agree with those of formamide in the ground state.

We used an LTE approximation (the lack of collisional rates for this molecule prevents a more detailed analysis). Nevertheless, taking into account the physical conditions of the considered component (see Sect. 4.2), we expect that this approximation works reasonably well.

We assumed uniform physical conditions for the kinetic temperature, density, radial velocity, and line width (see parameters quoted in Sect. 4.2). We adopted these values from the data analysis (Gaussian fits and an attempt to simulate the line profiles for several molecules with LTE and LVG codes in that line survey, see Tercero et al. 2010, 2011a) as representative parameters for the different cloud components. Our modelling technique also took into account the size of each component and its offset position with respect to IRc2. Corrections for beam dilution were applied to each line depending on their frequency. The only free parameter is therefore the column density. Taking into account

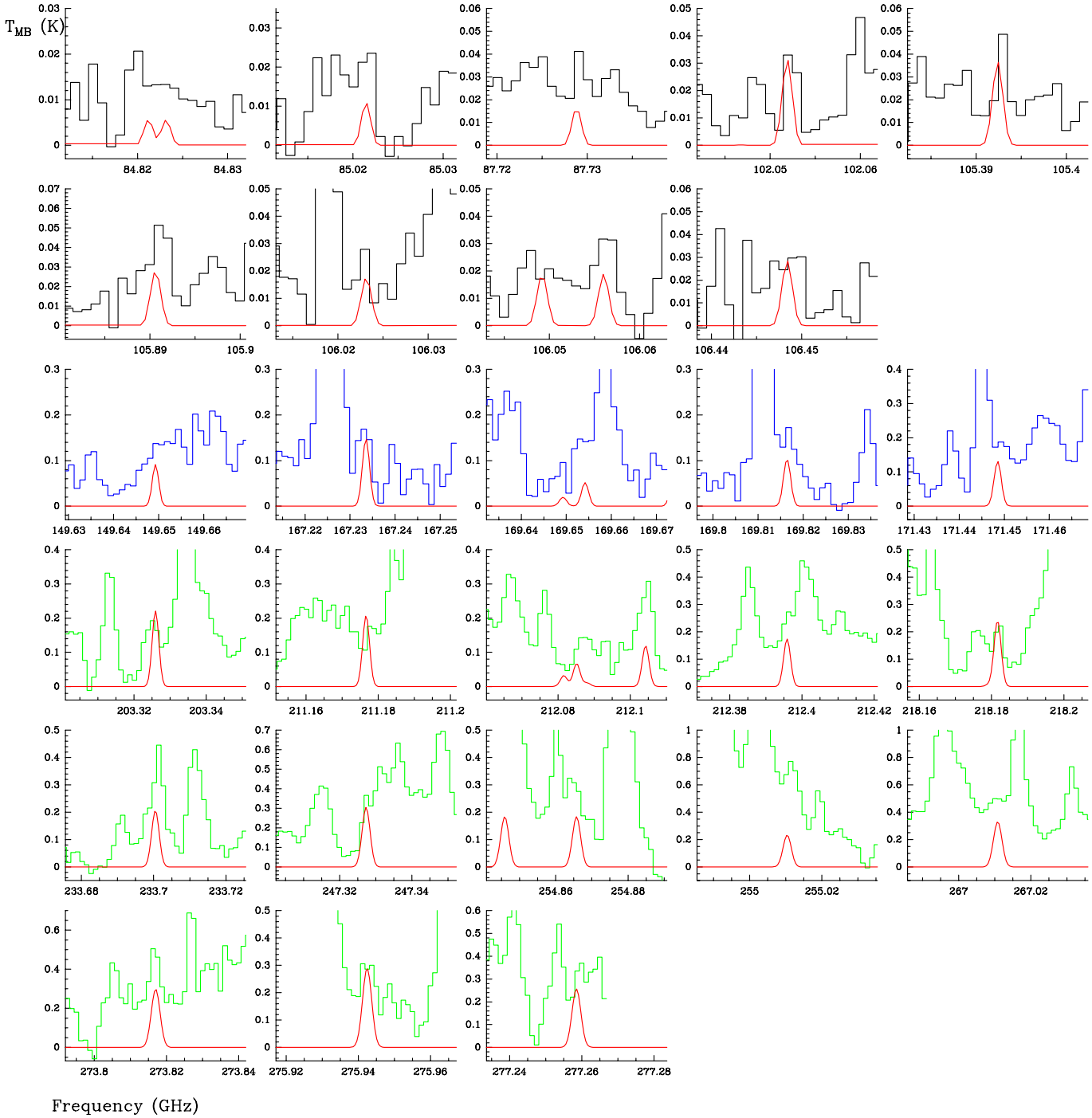

Fig. 1. Observed lines from Orion KL (histogram spectra in black, blue, and green for 3, 2 and 1.3 mm lines, respectively) and model (thin curves in red) of NH_2CHO $\nu_{12} = 1$. A v_{LSR} of 7.5 km s^{-1} is assumed.

the compact nature of the compact ridge and the hot core components, the contribution from the error beam is negligible. In addition to line opacity effects, we discussed other sources of uncertainty in Tercero et al. (2010). For the column density results, we estimated the uncertainty to be 25% for formamide in the ground state and, owing to the weakness of the observed lines, 50% for NH_2CHO $\nu_{12} = 1$.

For both components we assumed a source size of 10″ of diameter with uniform brightness temperature and optical depth over this size. The components are placed 7″ and 2″ from the pointed position for the compact ridge and the hot core, respectively. The column density results that reproduce the line profiles better are shown in Table 3.

Figure 1 and Table 2 show the comparisons between model and observations of vibrationally excited formamide lines. The differences between the intensity of the model and the peak intensity of the observed lines are mostly caused by the contribution of many other molecular species (the frequent overlap with other lines makes it difficult to provide a good baseline for the weak lines of vibationally excited formamide). Nevertheless, the observed line intensity of isolated detected lines of NH_2CHO $\nu_{12} = 1$ agrees with the model predictions.

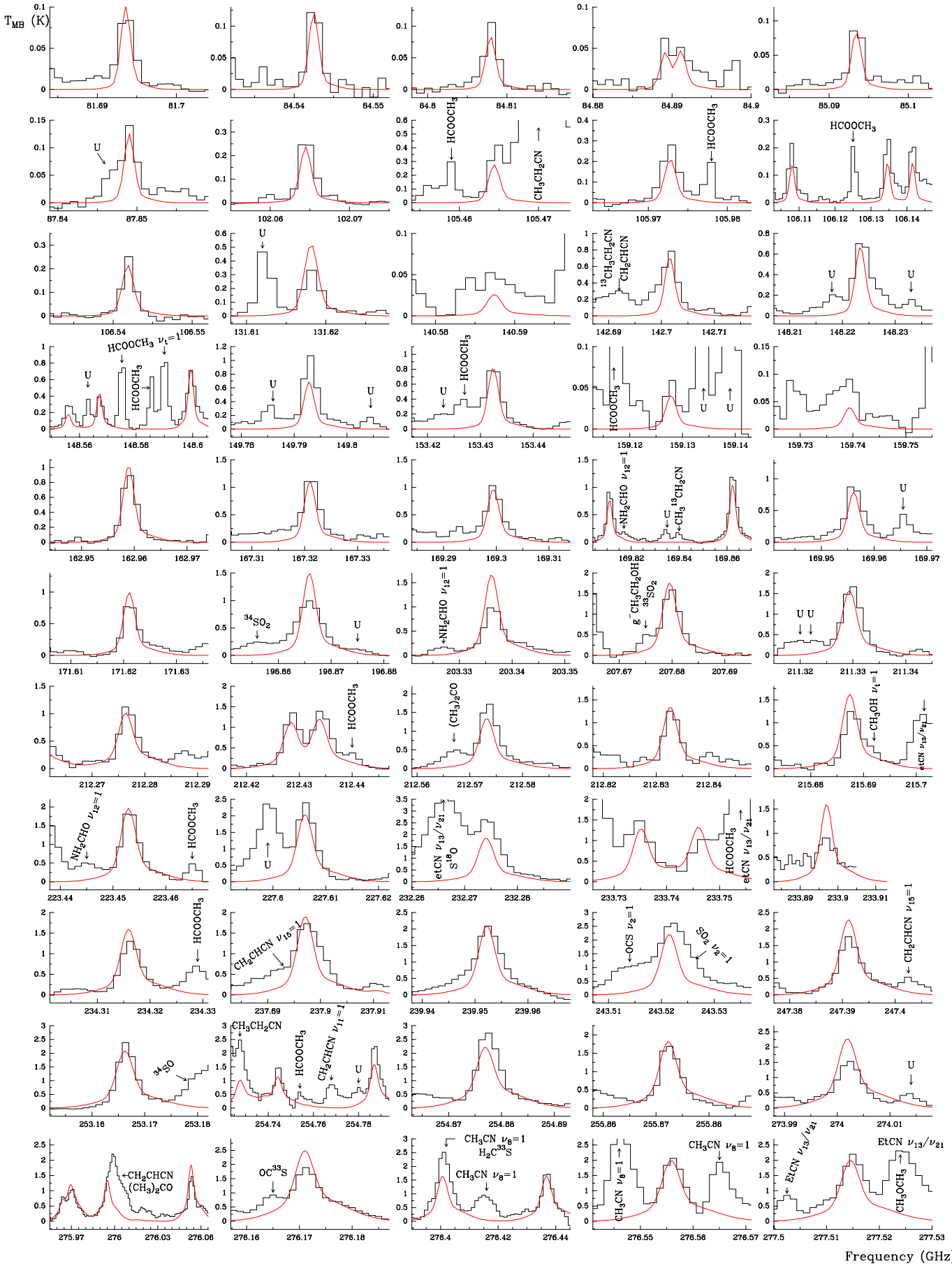

Fig. 2. Observed lines from Orion KL (histogram spectra in black) and model (thin curves in red) of NH_2CHO in the ground state. A v_{LSR} of 7.5 km s^{-1} is assumed.

Table 3. Column density results.

Species	$N_{\rm C.R.}$ cm^{-2}	$N_{\rm H.C.}$ cm^{-2}
NH_2CHO	$(7 \pm 2) \times 10^{14}$	$(6 \pm 2) \times 10^{14}$
NH_2CHO $\nu_{12} = 1$	$(7 \pm 4) \times 10^{13}$	$(6 \pm 3) \times 10^{13}$

Notes. Column density results for formamide.

4.4. Vibratonal temperatures

From the column density obtained for NH_2CHO in the ground and vibrationally excited state, we can estimate a vibrational temperature taking into account that

$$\frac{\exp\left(-\frac{E_{\nu_x}}{T_{\rm vib}}\right)}{f_\nu} = \frac{N(\mathrm{NH_2CHO}\ \nu_x)}{N(\mathrm{NH_2CHO})}, \quad (1)$$

where E_{ν_x} is the energy of the vibrational state ($E_{\nu_{12}} = 415.5$ K, $T_{\rm vib}$ is the vibrational temperature, f_ν is the vibrational partition function, $N(\mathrm{NH_2CHO}\ \nu_x)$ is the column density of the vibrational state, and $N(\mathrm{NH_2CHO})$ is the column density of formamide in the ground state. The vibrational partition function can be approximated by

$$f_\nu = 1 + \exp\left(-\frac{E_{\nu_3}}{T_{\rm vib}}\right) + 2\exp\left(-\frac{E_{\nu_2}}{T_{\rm vib}}\right) + \exp\left(-\frac{E_{\nu_1}}{T_{\rm vib}}\right), \quad (2)$$

which, for low $T_{\rm vib}$ leads to $f_\nu \simeq 1$.

From the observed lines, we obtain $T_{\rm vib} = 180 \pm 90$ K in both components. This value is the averaged kinetic temperature we adopted in our model: 110 and 250 K for the C.R. and the H.C., respectively. Hence, the LTE approximation can be considered a reasonable assumption.

A direct comparison of the derived $T_{\rm vib}$ for NH_2CHO with the average T_k assumed for the gas is difficult. Vibrational excitation is expected to depend strongly on temperature and density gradients in that region. It is also difficult to ascertain if either IR dust photons or molecular collisions dominate the vibrational excitation of NH_2CHO given the lack of collision rates for that species.

Nevertheless, since the vibrationally excited gas is not necessarily spatially coincident with the ground state gas, the derived vibrational temperatures have to be considered as lower limits.

5. Conclusions

We measured the rotational spectrum of formamide in the 400–950 GHz frequency range. The analysis was performed on the ground states of the parent and ^{13}C species as well as on the $\nu_{12} = 1$ excited vibrational state of the parent isotopologue of the molecule. Several tests performed in this study showed that both A- and S-reductions can be used for the analysis of the rotational spectra of formamide. A reliable set of obtained rotational parameters allows an accurate calculation of transition frequencies of formamide up to 1.5 THz for NH_2CHO and up to 1 THz for $NH_2^{13}CHO$.

Based on improved predictions available from the spectroscopic studies 55, spectral features that correspond to the $\nu_{12} = 1$ state of formamide were detected for the first time in the line survey of Orion KL with the IRAM 30-m telescope. The derived vibrational temperature indicates that LTE is a reasonable assumption in this case.

Acknowledgements. B.T. and J.C. thank the Spanish MICINN for support under grants AYA2006-14786, AYA2009-07304 and the CONSOLIDER program "ASTROMOL" CSD2009-00038. R.M. and L.M. would like to acknowledge the support of the Centre National d'Études Spatiales (CNES) and the French program "Action sur Projets de l'INSU, Physique et Chimie du Milieu Interstellaire".

Appendix A: Results of ab initio calculations on formamide

Table A.1. Ab initio rotational parameters for formamide (from the B3LYP/6+311+G(3df,2pd) calculation).

Parameter	Value	T_{gg}/B_g
A (MHz)	73 818.88	
B (MHz)	11 393.02	
C (MHz)	9869.75	
T_{aa} (kHz)	–1369.8	-7.5×10^{-5}
T_{bb} (kHz)	–10.916	-3.9×10^{-6}
T_{cc} (kHz)	–4.732	-1.9×10^{-6}
T_{ab} (kHz)	31.187	
T_{ac} (kHz)	27.362	
T_{bc} (kHz)	6.957	
$2R_5$ (kHz)	3.458	
R_6 (kHz)	–0.0108	
$s^{\rm A}_{111}$	2.9×10^{-7}	
$s^{\rm S}_{111}$	2.8×10^{-8}	

Notes. Parameters R_5, R_6, $s^{\rm A}_{111}$, $s^{\rm S}_{111}$ are calulated in I^r coordinate representation.

References

Alekseev, E. A., Motiyenko, R. A., & Margulès, L. 2012, Radio Phys. Radio Astron., 3, 75
Becke, A. D. 1988, Phys. Rev. A, 38, 3098
Blake, G. A., Sutton, E. C., Masson, C. R., & Philips, T. H. 1987, ApJ, 315, 621
Blake, G. A., Mundy, L. G., Carlstrom, J. E., et al. 1996, ApJ, 472, L49
Carvajal, M., Margulès, L., Tercero, B., et al. 2009, A&A, 500, 1109
Cernicharo 1985, Internal IRAM report (Granada: IRAM)
Costain, C. C., & Dowling, J. M. 1960, J. Chem. Phys., 32, 158
Demyk, K., Mäder, H., Tercero, B., et al. 2007, A&A, 466, 255
Johansson, L. E. B., Andersson, C., Elldér, J., et al. 1984, A&A, 130, 227
Johnson, D. R., Lovas, F. J., & Kirchhoff, W. H. 1972, J. Phys. Chem. Ref. Data, 1, 1011
Hirota, E., Sugisaki, R., Nielsen, C. J., & Sørensen, G. O. 1974, J. Mol. Spectrosc., 49, 251
Kirchhoff, W. H., & Johnson, D. R. 1973, J. Mol. Spectrosc., 45, 159
Kryvda, A. V., Gerasimov, V. G., Dyubko, S. F., Alekseev, E. A., & Motiyenko, R. A. 2009, J. Mol. Spectrosc., 254, 28
Kurland, R. J. 1955, J. Chem. Phys., 23, 2202
Kurland, R. J., & Bright Wilson, E., Jr. 1957, J. Chem. Phys., 27, 585
Lattelais, M., Pauzat, F., Ellinger, Y., & Ceccarelli, C. 2010, A&A, 519, A30
Lee, C., Yang, W., & Parr, R. G. 1988, Phys. Rev. B, 37, 785
Margulès, L., Motiyenko, R., Demyk, K., et al. 2009, A&A, 493, 565
Margulès, L., Huet, T. R., Demaison, J., et al. 2010, ApJ, 714, 1120
Morris, M., Palmer, P., & Zuckerman, B. 1980, ApJ, 237, 1
Moskienko, E. M., & Dyubko, S. F. 1991, Radiophys. Quant. Electron., 34, 181
Motiyenko, R. A., Margulès, L., Alekseev, E. A., Guillemin, J. C., & Demaison, J. 2010, J. Mol. Spectrosc., 264, 94
Pardo, J. R., Cernicharo, J., & Serabyn, E. 2001, IEEE Trans. Antennas and Propagation, 49, 1683
Pickett, H. M. 1991, J. Mol. Spectrosc., 148, 371
Rubin, R. H., Swenson, G. W., Jr., Benson, R. C., Tigelaar, H. L., & Flygare, W. H. 1971, ApJ, 169, L39
Tercero, B., Pardo, J. R., Cernicharo, & Goicoechea, J. R. 2010, A&A, 517, A96
Tercero, B., Vincent, L., Cernicharo, J., Viti, S., & Marcelino, N. 2011, A&A, 528, A26
Tercero, B., Margulès, L., Carvajal, M., et al. 2012, A&A, 538, A119
Vorob'eva, E. M., & Dyubko, S. F. 1994, Radiophys. Quant. Electron., 37, 155
Watson, J. K. G. 1977, Vibrational Spectra and Structure (Amsterdam: Elsevier)